How to cite: *Angew. Chem. Int. Ed.* **2021**, *60*, 3632–3639
International Edition: doi.org/10.1002/anie.202010690
German Edition: doi.org/10.1002/ange.202010690

Palladium-Oxo Clusters

Discovery and Supramolecular Interactions of Neutral Palladium-Oxo Clusters Pd_{16} and Pd_{24}

*Saurav Bhattacharya, Uttara Basu, Mohamed Haouas, Pei Su, Michael Forrester Espenship, Fei Wang, Albert Solé-Daura, Dereje H. Taffa, Michael Wark, Josep M. Poblet, Julia Laskin, Emmanuel Cadot, and Ulrich Kortz**

Abstract: *We report on the synthesis, structure, and physicochemical characterization of the first three examples of neutral palladium-oxo clusters (POCs). The 16-palladium(II)-oxo cluster $[Pd_{16}O_{24}(OH)_8((CH_3)_2As)_8]$ (**Pd_{16}**) comprises a cyclic palladium-oxo unit capped by eight dimethylarsinate groups. The chloro-derivative $[Pd_{16}Na_2O_{26}(OH)_3Cl_3((CH_3)_2As)_8]$ (**$Pd_{16}Cl$**) was also prepared, which forms a highly stable 3D supramolecular lattice via strong intermolecular interactions. The 24-palladium(II)-oxo cluster $[Pd_{24}O_{44}(OH)_8((CH_3)_2As)_{16}]$ (**Pd_{24}**) can be considered as a bicapped derivative of **Pd_{16}** with a tetra-palladium-oxo unit grafted on either side. The three compounds were fully characterized 1) in the solid state by single-crystal and powder XRD, IR, TGA, and solid-state ^1H and ^{13}C NMR spectroscopy, 2) in solution by ^1H, ^{13}C NMR and ^1H DOSY spectroscopic methods, and 3) in the gas phase by electrospray ionization mass spectrometry (ESI-MS).*

Introduction

Discrete metal-oxo clusters are an interesting class of compounds comprising metal ions connected via oxygen-based ligands (e.g. H_2O, OH^-, O^{2-}) with well-defined structure and chemical formula. The controlled self-assembly of such metal-oxo clusters of given shape, size and composition requires a precise control of hydrolysis and condensation phenomena.[1] This can primarily be achieved by the subtle manipulation of pH, concentration/type of metal ions, ionic strength, temperature, redox environment, and the judicious choice of the capping ligands that terminate cluster aggregations, which would otherwise lead to insoluble, amorphous mixtures of products. Over the years, extensive research has been undertaken in the areas of transition-metal and rare-earth-based metal-oxo/hydroxo clusters.[2–4] Such polynuclear complexes have been utilized extensively in the areas of band-gap tuning,[5] photocatalytic water-oxidation,[6] cryogenic magnetic cooling,[7] and single-molecular magnetism.[8] Moreover, metal-oxo clusters have also been utilized as secondary building units in the construction of purely inorganic 3D open-framework materials,[9] or metal–organic frameworks (MOFs),[10] which in turn have shown immense promise as heterogeneous photo-/electrocatalysts and as gas-separating agents.

One of the most important subclasses of discrete metal-oxo clusters are polyoxometalates (POMs), which are polynuclear anions typically composed of early *d*-block metal ions in high oxidation states, such as W^{VI}, Mo^{VI}, and V^V, linked by oxo ligands.[11] The area of POMs encompasses a uniquely diverse range of molecular metal-oxo clusters with a multitude of compositions, shapes, and sizes. Their high solution, thermal and photo/electrochemical stability render them highly attractive species for applications in catalysis, magnetism, and molecular electronics.[12] Furthermore, POMs can be covalently coordinated or electrostatically associated with other cations or cationic polynuclear complexes to form composite or supramolecular assemblies.[13]

Following Döbereiner's idea that noble-metal-based oxo-clusters with well-defined structures can be used as models to decode the intrinsic molecular mechanism of noble-metal-based catalysis,[14] extensive research has been undertaken to synthesize noble-metal-based POMs (with noble-metal ions as addenda). In 2004, Wickleder's group discovered the first polyoxo-12-platinate(III), $[Pt^{III}_{12}O_8(SO_4)_{12}]^{4-}$.[15] Following this, Kortz's group reported the first polyoxopalladate(II) (POP), $[Pd_{13}As_8O_{34}(OH)_6]^{8-}$ in 2008, as well as the first polyoxoaurate(III), $[Au^{III}_4As^V_4O_{20}]^{8-}$ in 2010, which eventu-

[*] Dr. S. Bhattacharya, Dr. U. Basu, Prof. U. Kortz
Department of Life Sciences and Chemistry, Jacobs University
Campus Ring 1, 28759 Bremen (Germany)
E-mail: u.kortz@jacobs-university.de
Dr. M. Haouas, Prof. E. Cadot
Institut Lavoisier de Versailles, CNRS, UVSQ, Université Paris-Saclay
Versailles (France)
P. Su, M. F. Espenship, Prof. J. Laskin
Department of Chemistry, Purdue University
560 Oval Drive, West Lafayette, IN 47907 (USA)
F. Wang, Dr. A. Solé-Daura, Prof. J. M. Poblet
Departament de Química Física i Inorgànica
Universitat Rovira i Virgili
Marcel lí Domingo 1, 43007 Tarragona (Spain)
Dr. D. H. Taffa, Prof. M. Wark
Institute of Chemistry, Carl von Ossietzky University Oldenburg
26129 Oldenburg (Germany)
Supporting information and the ORCID identification number(s) for the author(s) of this article can be found under: https://doi.org/10.1002/anie.202010690.

© 2020 The Authors. Angewandte Chemie International Edition published by Wiley-VCH GmbH. This is an open access article under the terms of the Creative Commons Attribution Non-Commercial NoDerivs License, which permits use and distribution in any medium, provided the original work is properly cited, the use is non-commercial and no modifications or adaptations are made.

ally led to the discovery of several other noble-metal and mixed noble-metal ion-based POMs having different shapes, sizes and compositions.[16–19] POPs, in general, have also shown immense promise as noble-metal-based homogeneous and heterogeneous catalysts.[16b,17] Noble-metal ions other than Pd^{II} and Au^{III} have also been utilized to synthesize metal-oxo clusters.[20] Most of the noble-metal-oxo clusters reported are either anionic or cationic, with only very few examples of neutral clusters. Some neutral Ti^{IV} and Zr^{IV}-based oxo-clusters with the general formula $M_xO_y(OH)_z(RCOO)_n$ ($M = Ti^{IV}$, Zr^{IV}) are known, wherein the metal-oxo/hydroxo clusters are capped by monoanionic, bidentate carboxylate groups.[3a–e] Very recently, neutral Al^{III}-oxo clusters have been reported with the general formula $Al(OH)_x(OR)_y(R'OOCPh)_{3-x-y}$.[3f] A similar strategy was employed recently to isolate a neutral Ru^{III}-based oxo-cluster.[21] Herein, we report on the synthesis, structure and characterization of the first discrete and neutral polyoxopalladium clusters.

Results and Discussion

Synthesis and Structure

The novel discrete, neutral polyoxo-16-palladium(II) cluster $[Pd_{16}O_{24}(OH)_8((CH_3)_2As)_8]$ (**Pd_{16}**) was synthesized by room-temperature stirring of a mixture of palladium(II) acetate $Pd(OAc)_2$ in a sodium dimethylarsinate (also known as cacodylate, from here on abbreviated as cac) buffer solution at pH 7 for 2 days (after reaction pH was ≈5.7), followed by filtration and crystallization (see Supp. Info for Exp. Section). Single-crystal X-ray analysis revealed that the **Pd_{16}** comprises 16 square-planar oxo-coordinated palladium-(II) ions, which can be subdivided in a central $[Pd_8O_8(OH)_8]^{8-}$ square-antiprismatic unit, encircled by a cyclic $[Pd_8O_{16}((CH_3)_2As)_8]^{8+}$ unit, resulting in the neutral, discrete metal-oxo cluster **Pd_{16}** (Figure 1). All Pd^{2+} ions in **Pd_{16}** exhibit a square-planar coordination geometry with Pd-O distances in the range of 1.978(9)–2.053(9) Å (Supporting Information, Table S2). The novel **Pd_{16}** has idealized D_{4d} point group symmetry with the C_4 principal rotation axis passing through the central $[Pd_8O_8(OH)_8]^{8-}$ square-antiprismatic unit. Bond valence sum (BVS) calculations on the μ_2-OH groups yields values of 1.02–1.16 (Table S4), confirming that these oxygens are monoprotonated. To the best of our knowledge, this is the first example of a discrete, neutral Pd-oxo cluster. To date, only a handful of neutral noble-metal-based oxo-clusters have been reported.[21]

In the solid-state lattice, each **Pd_{16}** is further linked through weak C–H···O hydrogen bonds to other **Pd_{16}** units (as well as to the co-crystallized cacodylates) to form a supramolecular 2D layered assembly (Supporting Information, Figure S1, Table S5). This labile supramolecular arrangement of **Pd_{16}** results in high solubility of the compound in water. In fact, the crystalline nature of the material is lost rapidly upon filtration and exposure to air turning it amorphous.

The second novel discrete palladium(II)-oxo cluster $Na_2[Pd_{16}O_{26}(OH)_3Cl_3((CH_3)_2As)_8]$ (**$Pd_{16}Cl$**) was synthesized by room-temperature stirring of a mixture of palladium(II) chloride $PdCl_2$ in a sodium cacodylate buffer solution at pH 7 for 2 days (after reaction pH was ≈5.7), followed by filtration and crystallization (see Supp. Info for Exp. Section). Single-crystal X-ray analysis demonstrated that **$Pd_{16}Cl$** has an overall identical structure as **Pd_{16}**, but careful analysis revealed the presence of some chloro ligands. The use of palladium(II) chloride (rather than acetate) resulted in partial substitution of the μ_2-OH groups O1A, O2A, O3A, and O4A (each having a crystallographic *sof* of 0.625) by Cl^- (Cl1, Cl2, Cl3 and Cl4 each having a crystallographic *sof* of 0.375). Thus, the structure of **$Pd_{16}Cl$** can be described as a central $[Pd_8O_{10}(OH)_3Cl_3]^{10-}$ square-antiprismatic unit encircled by a ring-shaped $[Pd_8O_{16}((CH_3)_2As)_8]^{8+}$ unit, leading to the formation of a discrete dianionic assembly $[Pd_{16}O_{26}(OH)_3Cl_3((CH_3)_2As)_8]^{2-}$ (Figures 2 (left); Figure S2). Elemental analysis indicated that this negative charge is balanced by two sodium counter cations, which could not be located by single-crystal XRD due to disorder. Nonetheless, their presence was also suggested by theoretical computations (vide infra). However, ESI-MS studies (vide infra) indicate that in solution, the two deprotonated hydroxo groups reprotonate, yielding the neutral free acid **$H_2Pd_{16}Cl$**. In essence, the main differences between **$Pd_{16}Cl$** and **Pd_{16}** are that in the former (i) three hydroxo groups are replaced by Cl^- ions and (ii) two of the hydroxo groups are deprotonated and the negative charge is balanced by two Na^+ ions. The presence of a strong hydrogen bond acceptor in the form of Cl^- in **$Pd_{16}Cl$** leads to strong C–H···Cl interactions involving the μ_2-OH/Cl^- groups (O1A/Cl1, O2A/Cl2, O3A/Cl3, O4A/Cl4) and the C–H bonds of the cacodylate methyl groups (Table S9, Figure S2).[22] Furthermore, the introduction of the Cl^- groups introduces a certain degree of hydrophobicity in **$Pd_{16}Cl$** (see the computational study in the proceeding text), which in turn

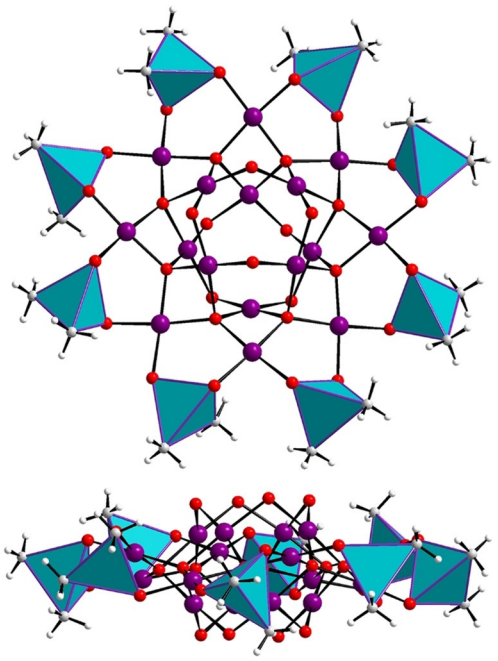

Figure 1. Structural representation of the disk-shaped **Pd_{16}**; (top) top view and (bottom) side view. Color code: Pd (violet), O (red), C (gray), H (white), $(CH_3)_2AsO_2$ (cyan tetrahedra).

 © 2020 The Authors. Angewandte Chemie International Edition published by Wiley-VCH GmbH

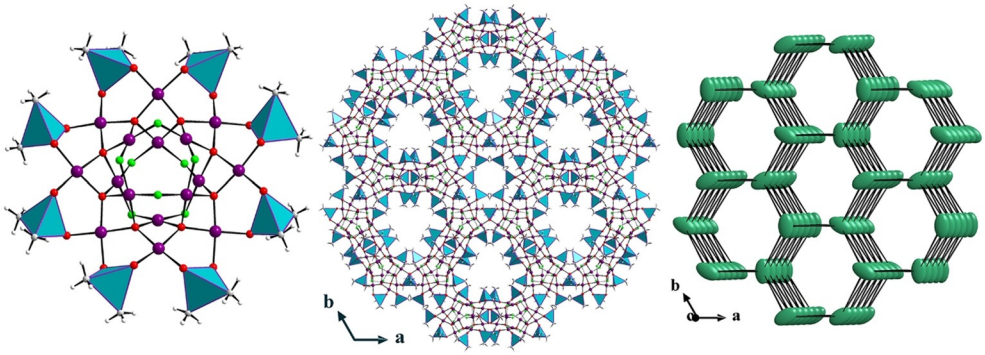

Figure 2. (left) Structural representation of the disk-shaped **$Pd_{16}Cl$**. Color code: Pd (violet), Cl/O (disordered; light-green), O (red), C (gray), H (white), $(CH_3)_2AsO_2$ (cyan tetrahedra). (middle) 3D lattice structure of **$Pd_{16}Cl$**. (right) Uninodal acs topology in **$Pd_{16}Cl$**. The dark-green ellipsoids represent individual **$Pd_{16}Cl$** units.

leads to stronger intermolecular interactions in 3D space. Thus, each **$Pd_{16}Cl$** unit is linked to six others leading to a stable 3D hydrogen-bonded organic–inorganic framework (HOIF). This 3D arrangement exhibits a uninodal *acs* framework topology featured by the Schläfli symbol $4^9.6^6$,[23] giving rise to hexagonal 1D-channels running along the "*c*" direction (Figure 2). There are only a handful of such types of frameworks reported in the literature, probably due to the inherent difficulty of controlling hydrogen bond interactions between the organic and inorganic components.[24] **$Pd_{16}Cl$** is the first such example of a noble-metal-oxo-cluster-based 3D HOIF. The formation of a stable 3D framework in **$Pd_{16}Cl$** is accompanied by a higher isolated yield and crystallinity as well as lower aqueous solubility as compared to **Pd_{16}**.

The stability and crystallinity of **$Pd_{16}Cl$** was further corroborated by PXRD studies (Figure 3 (top)). The PXRD pattern of freshly prepared **$Pd_{16}Cl$** matched well with the simulated PXRD pattern, indicating phase-purity. Upon dehydration of **$Pd_{16}Cl$** by heating to 70 °C for 1 h, only minimal changes were observed in the PXRD pattern, indicating that even upon loss of the lattice water molecules, the framework retains its stability and long-range order. Rehydration in a wet atmosphere at room temperature again keeps the PXRD spectrum intact. Thermogravimetric analysis (TGA) studies on **$Pd_{16}Cl$** reiterated the stability of the compound upon dehydration and rehydration (Figure 3 (bottom); Supporting Information). Thus, the introduction of Cl^- ions into the **Pd_{16}** induces a drastic improvement in the stability and crystallinity of the compound due to the formation of stable extended supramolecular assembly.

The third novel discrete, neutral palladium(II)-oxo cluster $[Pd_{24}O_{44}(OH)_8((CH_3)_2As)_{16}]$ (**Pd_{24}**) was synthesized by room-temperature stirring of a mixture of palladium(II) acetate $Pd(OAc)_2$ in a sodium cacodylate buffer solution at pH 7 for 2 days (after reaction pH was ≈5.8), followed by adjustment of pH to ≈7 by $NaOH_{aq}$ solution and then stirred further for 1 day before filtering. This step is crucial because without such pH readjustment after the reaction **Pd_{16}** is formed. Attempts to synthesize a chloro-derivative of **Pd_{24}** by adjusting the pH of the reaction mixture of **$Pd_{16}Cl$** to ≈7 after 2 days of stirring at room temperature failed, and instead **$Pd_{16}Cl$** was obtained in low yield. The structure of **Pd_{24}** contains **Pd_{16}** as a core, but then four of the eight μ_2-hydroxo groups (two on either side of the molecule) are deprotonated and bind to two cationic, tetranuclear $[Pd_4O_8(OH)_2((CH_3)_2As)_4]^{2+}$ units, one on each side of the cluster, resulting in the bicapped $[Pd_{24}O_{44}(OH)_8((CH_3)_2As)_{16}]$ (**Pd_{24}**) (Figure 4; Figure S3). **Pd_{24}** has idealized point group symmetry C_1 and crystallizes in the triclinic space group $P\bar{1}$ (Table S1). The deprotonation step appears to be the key for the formation of **Pd_{24}** and this is accomplished by pH 7 adjustment after reaction. The bond valence sum (BVS) calculations on the μ_2-OH groups yield values of 1.08–1.18 (Table S12), which are typical for hydroxo groups. In the solid state, each **Pd_{24}** cluster is further linked to four other **Pd_{24}** clusters through weak C–H···O interactions involving the C–H bonds of the methyl groups, the oxygens of the cacodylates and the μ_2-OH groups, resulting in a 4-connected hydrogen-bonded SBU (Figure S4, Table S13). This leads to a 3D HOIF with a *dia* topology with the Schläfli symbol 6^6.[25] However, in spite of forming such a framework, the weak C–H···O hydrogen bonds impart

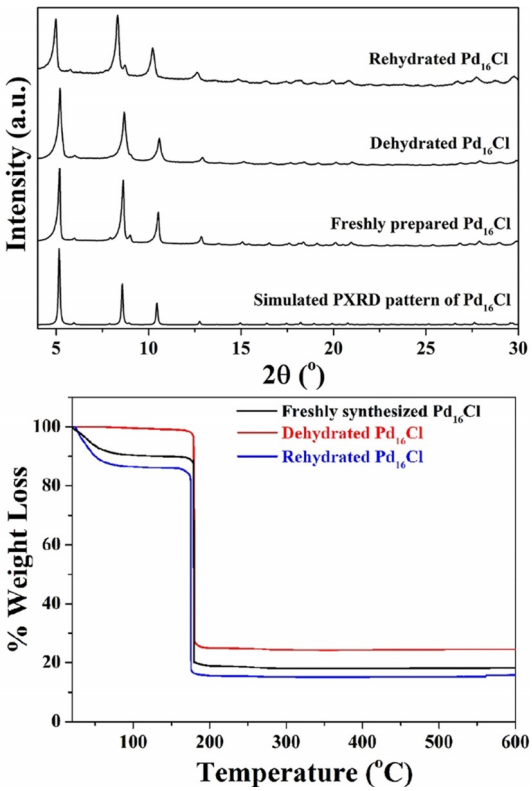

Figure 3. (top) PXRD patterns and (bottom) TGA curves of freshly prepared, dehydrated, and rehydrated compound **$Pd_{16}Cl$**.

 © 2020 The Authors. Angewandte Chemie International Edition published by Wiley-VCH GmbH

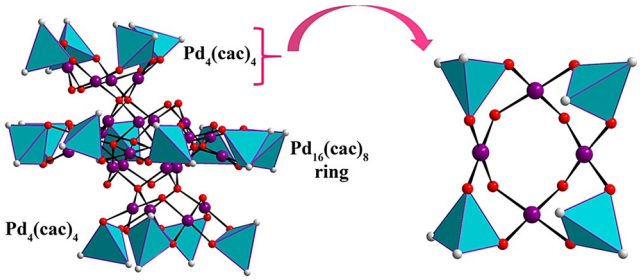

Figure 4. Structural representation of **Pd_{24}**, which can be viewed as a bicapped **Pd_{16}**. Color code: Pd (violet), O (red), C (gray), $(CH_3)_2AsO_2$ (cyan tetrahedra). Hydrogen atoms are omitted for clarity.

significant lability and flexibility to the 3D assembly leading to the loss of crystallinity upon exposure to air and high aqueous solubility (Figure S4d).

Solid-state, Solution, and DOSY NMR Spectroscopy

Although the molecular entities of **$Pd_{16}Cl$** and **Pd_{16}** are isostructural, the former has a significantly higher yield and therefore it was utilized for NMR measurements. The ^{1}H 30 kHz MAS spectrum of cacodylic acid (H-cac) exhibits two broad peaks at ≈1.8 and ≈12.3 ppm, corresponding to the protons of the methyl and those of the acidic groups, respectively (Figure 5 (top)). The broadness of the peaks reflects a strong H-H dipolar interaction between the different cacodylic acid molecules stacked in the crystal structure, which is typical for small organic molecules.[26] The ^{1}H 30 kHz MAS spectrum of the sodium salt of cacodylic acid (Na-cac), however, exhibits two sharp peaks at ≈1.6 and ≈5.3 ppm, corresponding to the protons of the methyl groups and the crystal water molecules, respectively. The sharpness of the peaks is due to the fact that sodium cacodylate liquefies itself in its water of crystallization at ca 60 °C, leading to a solution-like behavior.[27a] Indeed, the high spinning frequency (ca 30 kHz) is known to induce sample heating during solid-state NMR experiments (the estimated temperature inside the NMR rotor is ≈57 °C at 30 kHz).[27b] This was further proven by ^{1}H MAS NMR spectroscopy of Na-cac at spinning frequencies below 20 kHz, which resulted in broad peaks at ≈1.2 and ≈5.9 ppm, respectively (Figure 5 (top); Figure S6a). The ^{1}H solid-state NMR spectra of **$Pd_{16}Cl$** and **Pd_{24}** reveal broad peaks at ≈2.4 and ≈1.9 ppm, respectively, corresponding to the protons of the cacodylate methyl groups. In addition, a small peak at −0.7 ppm is observed for **Pd_{24}**, which corresponds to the protons of the μ_2-OH groups.[28] A similar peak is not observed in the ^{1}H-solid-state spectrum of freshly prepared **$Pd_{16}Cl$**, probably due to fast exchange of these protons with the lattice water molecules. Indeed, upon thermal dehydration at 100 °C for 2 hours, a small peak at −1.9 ppm corresponding to the μ_2-OH groups is now visible in the spectrum, indicating a frozen regime after complete removal of the lattice water molecules (Figure 5 (bottom)). The situation is different for **Pd_{24}**, where some of the μ_2-OH groups are located in hydrophobic pockets lined by the cacodylate groups, which prevents such an exchange regime

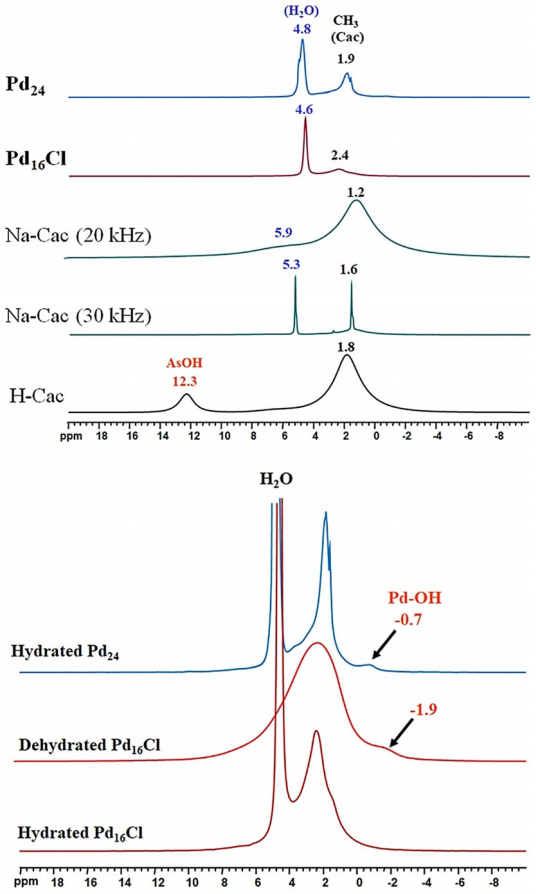

Figure 5. (top) ^{1}H MAS NMR (30 kHz) spectra of **$Pd_{16}Cl$** and **Pd_{24}** compared to spectra of cacodylic acid (H-cac) and its sodium salt (Na-cac, rotation speeds 20 and 30 kHz) as references. (bottom) ^{1}H MAS NMR (30 kHz) spectra of as-prepared (hydrated) **$Pd_{16}Cl$** and **Pd_{24}**, as well as a thermally dehydrated (100 °C for 2 h) **$Pd_{16}Cl$** sample.

(Figure 4). In the solid state, the ^{1}H NMR peak corresponding to the hydroxo group can span a wide window depending on the extent of hydrogen bonding with acceptor molecules such as water and therefore, in turn, the extent of shielding–deshielding. Finally, we note the absence of the deshielded signal (12.3 ppm) due to the acidic proton indicating the complete deprotonation of the cac ligands in **$Pd_{16}Cl$** and **Pd_{24}**.

The ^{13}C{^{1}H} CPMAS (10 kHz) solid-state NMR spectrum of H-cac exhibits two narrow peaks at 15.6 and 20.3 ppm that correspond to the two crystallographically inequivalent cacodylic acid molecules present in the crystal structure of cacodylic acid (Figure 6).[26] The ^{13}C solid-state NMR spectrum of Na-cac also exhibits two peaks at 19.3 and 19.9 ppm for the same reason.[26] The ^{13}C solid-state NMR spectra of **$Pd_{16}Cl$** and **Pd_{24}**, however, exhibit multiple overlapping broad peaks in the region 18–28 ppm and 15–30 ppm, respectively. These resonances could be attributed to the presence of 5 (**$Pd_{16}Cl$**) and 16 (**Pd_{24}**) crystallographically inequivalent cacodylates in their respective single crystal structures, which leads to several unresolved NMR lines of the methyl groups (Figure 6).

 © 2020 The Authors. Angewandte Chemie International Edition published by Wiley-VCH GmbH

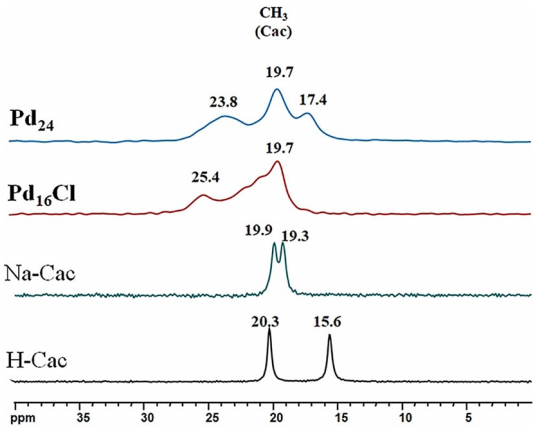

Figure 6. $^{13}C\{^1H\}$ CPMAS NMR (10 kHz) spectra of **$Pd_{16}Cl$** and **Pd_{24}** compared to spectra of cacodylic acid (H-cac) and its sodium salt (Na-cac) as references.

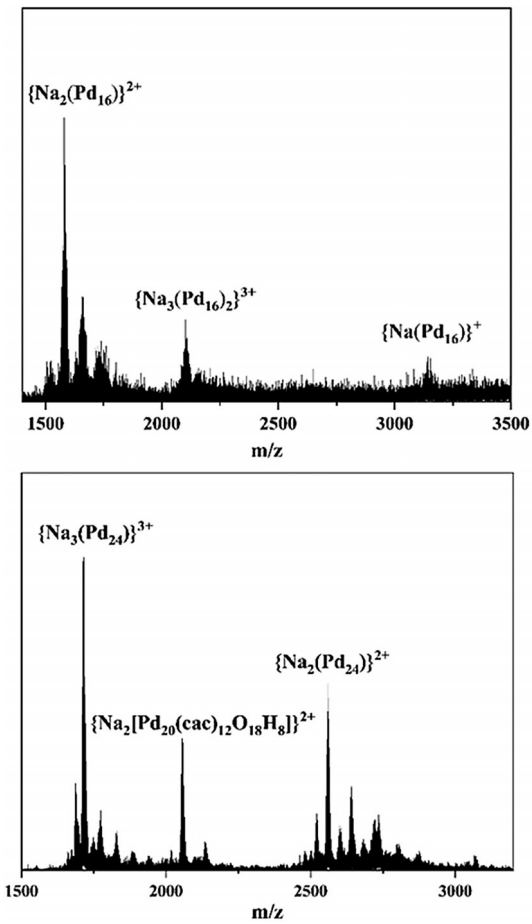

Figure 7. ESI-MS spectra of (top) **$Pd_{16}Cl$** and (bottom) **Pd_{24}**. Major species labeled in the Figure correspond to singly, doubly, and triply sodiated **$Pd_{16}Cl$** and **Pd_{24}** clusters, respectively, as well as to a partially dissociated species of **Pd_{24}**.

The ^1H (D_2O) liquid-state NMR spectra of H-cac and Na-cac exhibit sharp peaks at 1.9 and 1.6 ppm, respectively, corresponding to the protons of the methyl groups (Figure S6b). The low solubility of **$Pd_{16}Cl$** in water prevented us from acquiring a proper ^1H-NMR spectrum. The ^1H (D_2O) NMR spectrum of **Pd_{24}**, however, exhibits peaks at 1.6 and 1.8 ppm that correspond to the co-crystallized cacodylate and acetate, respectively, and a set of resonances in the region 1.7–3.1 ppm that likely corresponds to the methyl protons of the coordinated cacodylates in **Pd_{24}** (Figure S6b). The ^1H-DOSY NMR spectrum of **Pd_{24}** (Figure S7) confirms these assignments where the signal of acetate (1.8 ppm) indicates a diffusion coefficient D of 840 $\mu m^2 s^{-1}$, and the free cacodylate signal (1.6 ppm) a value of 670 $\mu m^2 s^{-1}$, comparable to that of Na-cac observed at 640 $\mu m^2 s^{-1}$. All other small peaks (1.7–3.1 ppm) are aligned around a value of D 215 $\mu m^2 s^{-1}$. Such a decrease of D by a factor of around three is fully consistent with coordination of the cac ligands to a nanoscopic object, such as **Pd_{24}**.

Mass spectrometry. All the peaks observed in the ESI-MS spectrum of **$Pd_{16}Cl$** could be clearly assigned to molecular species related to the neutral free acid form of the 16-palladium-oxo cluster (Figure 7 (top); Table S14a and experimental and simulated isotope distributions in Figure S8a), with the main peak at $m/z = 1581.496$ corresponding to the species $\{Na_2[Pd_{16}O_{24}(OH)_5Cl_3((CH_3)_2As)_8]\}^{2+}$ (denoted as $\{Na_2(Pd_{16})\}^{2+}$), the peak at $m/z = 2101.329$ corresponding to the species $\{Na_3(Pd_{16})_2\}^{3+}$, and the peak at $m/z = 3140.006$ corresponding to $\{Na(Pd_{16})\}^{+}$. Thus, the ESI-MS spectrum of **$Pd_{16}Cl$** corroborates the solid-state structural analysis. Similarly, the ESI-MS spectrum of **Pd_{24}** (Figure 7 (bottom); Table S14b and experimental and simulated isotope distributions in Figure S8b) exhibits peaks that can be clearly assigned to the molecular species related to the 24-palladium-oxo cluster, with the main peak at $m/z = 1713.991$ corresponding to $\{Na_3[Pd_{24}O_{44}(OH)_8((CH_3)_2As)_{16}]\}^{3+}$ (denoted as $\{Na_3(Pd_{24})\}^{3+}$) and the peak at $m/z = 2559.988$ corresponding to $\{Na_2(Pd_{24})\}^{2+}$. The peak at $m/z = 2057.769$ is consistent with a partially dissociated species having the formula $\{Na_2[Pd_{20}O_{10}(OH)_8((CH_3)_2AsO_2)_{12}]\}^{2+}$ (Table S14b), which indicates the fragility of the **Pd_{24}**-moiety in the gas-phase. We can envisage this partially dissociated species to be formed by removal of one of the $Pd_4(cac)_4$ capping units from one side of the $Pd_{16}(cac)_8$ (Figure 4).

Computational Studies on Pd_{16} and $Pd_{16}Cl$

We carried out atomistic MD simulations with explicit solvent molecules to compare the behavior in solution of **Pd_{16}** and the dianionic form **$Pd_{16}Cl$** with an aim to provide an explanation for the different supramolecular assemblies observed in the X-ray crystal structures of both species and their significantly different aqueous solubility. To do so, we simulated 15 **Pd_{16}** clusters and 15 **$Pd_{16}Cl$** anions, with their respective Na^+ counter cations for 250 ns and analyzed their collective behavior. Visual exploration of the MD trajectories revealed that, at a cluster concentration of ca. 90 mM, both species are capable of forming large agglomerate structures in a similar manner, although of a different nature. Figure 8 compares the **Pd_{16}**···**Pd_{16}** radial distribution functions (RDFs) for the simulated systems. The distribution of **Pd_{16}** around each other (Figure 8a (red line)) shows a main peak that

 © 2020 The Authors. Angewandte Chemie International Edition published by Wiley-VCH GmbH

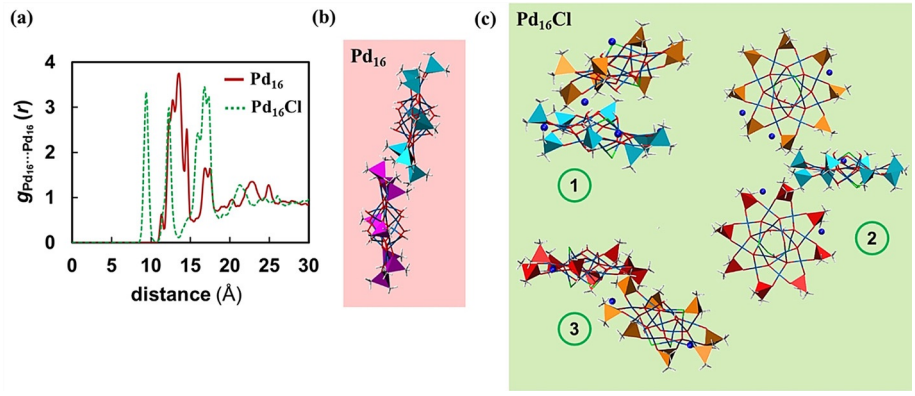

Figure 8. a) Radial distribution function (RDF) between **Pd_{16}** clusters taking the respective centers of mass as reference, averaged over the last 10 ns of a 250 ns simulation and over 15 clusters, with data sampling every 2 ps. The red solid line corresponds to **Pd_{16}** whereas the green dashed line corresponds to the sodium salt of the dianionic form of **$Pd_{16}Cl$**. b,c) Representative snapshots associated with the maxima of the RDFs, representing agglomerated species formed during the simulations with **Pd_{16}** (b) and **$Pd_{16}Cl$** (c). The cacodylate moieties of different clusters are represented in different colors for clarity, and sodium cations are shown as blue spheres.

covers an array of distances between ca. 12 and 14.5 Å, indicating that these are the preferred intermolecular distances for the **Pd_{16}**···**Pd_{16}** interactions in solution. This corresponds to an interaction mode in which the clusters bring together the methyl groups of their respective cacodylate moieties (Figure 8b) and thus, it can be classified as a hydrophobic interaction. In addition, the clusters tend to interact in a kind of layered disposition that resembles the one observed in the crystal (Figure S1). Other observed contacts correspond to interactions of the same nature, although less structured or involving three or more clusters (Figure S10). Conversely, **$Pd_{16}Cl$** anions do not show such preference for interacting in a single fashion, but the RDF indicates three well-differentiated interaction modes (Figure 8a (green dashed line)), represented in Figure 8c. Notably, this is in good agreement with three different interaction modes observed in the trigonal crystal structure, in which every dianion is surrounded by six neighbors (Figure S2). Thus, it is reasonable to think that the formation of these agglomerates can be related to the initial nucleation steps towards the crystal formation, as previously observed in MD simulations with Wells-Dawson-type heteropolytungstate ions.[29] It is also worth mentioning that unlike the dianionic cluster, the protonated form of **$Pd_{16}Cl$** exhibits intercluster interactions that do not differ significantly from those observed for **Pd_{16}** (Figure S11), in agreement with the fact that **$Pd_{16}Cl$** has to lose two protons during the crystallization process to yield a different supramolecular assembly than **Pd_{16}** (trigonal $P\bar{3}c1$ vs. triclinic $P\bar{1}$ crystal structures, vide supra). Moreover, these simulations also served to identify the most likely positions for the Na^+ ions in the crystal structure of **$Pd_{16}Cl$**, which could not be determined by X-ray diffraction. As shown in the volumetric densities of Figure S12, the sodium cations tend to sit between the oxygen atoms of vicinal cacodylate groups. Considering the vast number of equivalent sites, one might not expect that the X-ray crystal structure can show a single preferred position for them with high occupancy.

We performed another set of MD simulations with one cluster each of **Pd_{16}**, **$Pd_{16}Cl$** and the protonated form **$H_2Pd_{16}Cl$** (expected to be the dominant species in solution) in water to determine the distribution of water molecules around each cluster and the strength of their interactions (Figure S13 and associated text, Table S15). The different interaction modes of **Pd_{16}** and **$Pd_{16}Cl$** can be ascribed to an increasing hydrophobicity of the inner Pd_8 core in moving from **Pd_{16}** to the Cl-containing **$Pd_{16}Cl$**. Therefore, the core of **$Pd_{16}Cl$** might be more prone to interacting with the hydrophobic methyl groups of other clusters, whereas the more hydrophilic core of **Pd_{16}** with 8 hydroxo ligands is more likely surrounded by water molecules available, with which it can establish a greater number of hydrogen bonds. The comparison of the Pd_{16}···water RDFs represented in Figure S13 suggests that indeed, the incorporation of chloride ligands in the structure prevents the association of water molecules and, in consequence, can modulate the 3D structure of the supramolecular assembly incurred upon crystallization. In fact, this is not surprising since synthesis of chloride- and other halide-containing molecules has been extensively employed as a strategy to enhance the hydrophobicity of organic drugs and in turn, their membrane penetration in cells and binding to pathological proteins.[30]

Conclusion

We have discovered the first set of discrete and neutral polyoxopalladium clusters (POCs): the 16-palladium(II)-oxo cluster $[Pd_{16}O_{24}(OH)_8((CH_3)_2As)_8]$ (**Pd_{16}**) as well as its bicapped derivative, the 24-palladium(II)-oxo cluster $[Pd_{24}O_{44}(OH)_8((CH_3)_2As)_{16}]$ (**Pd_{24}**). Partial substitution of the OH^- groups in **Pd_{16}** by Cl^- groups resulted in $[Pd_{16}Na_2O_{26}(OH)_3Cl_3((CH_3)_2As)_8]$ (**$Pd_{16}Cl$**), which forms a highly stable 3D supramolecular lattice via strong intermolecular interactions, representing the first noble-metal-cluster-based stable and crystalline 3D hydrogen-bonded organic–inorganic framework (HOIF). All three novel palladium-oxo clusters **Pd_{16}**, **$Pd_{16}Cl$** and **Pd_{24}** were prepared by simple open-pot, room-temperature reactions of palladium(II) salts in sodium cacodylate solutions along with subtle pH adjustments, and they were characterized in the solid state by single-crystal and powder XRD, IR, TGA, and solid-state ^1H and ^{13}C NMR spectroscopic methods, in solution by ^1H, ^{13}C NMR, and ^1H DOSY spectroscopy, and in the gas phase by electrospray ionization mass spectrometry (ESI-MS). The discovery of the first three neutral palladium(II)-oxo clusters **Pd_{16}**, **$Pd_{16}Cl$**, and **Pd_{24}** is related to using a new type of capping group, dimethylarsinate (cacodylate), which acts as a bidentate,

 © 2020 The Authors. Angewandte Chemie International Edition published by Wiley-VCH GmbH

monoanionic ligand for the palladium-oxo core. So far only anionic palladium-oxo clusters were known (polyoxopalladates, POPs) and therefore the discovery of neutral palladium-oxo clusters (POCs) represent a breakthrough in noble metal-oxo chemistry. We have evidence that **Pd_{16}**, **$Pd_{16}Cl$**, and **Pd_{24}** are only the first three members of a large family of cacodylate-capped, neutral POCs. It is likely that other noble metals such as gold or platinum form discrete metal-oxo cores with cacodylate capping groups. The first three POCs reported herein serve as new model systems for studying noble-metal-based catalysis and can be considered as bottom-up precursors for the formation of noble-metal nanoparticles with controlled particle sizes and nuclearities.[3b,31] All the aforementioned studies are currently ongoing in our laboratory.

Acknowledgements

U.K. thanks the German Research Council (DFG, KO-2288/26-1), Jacobs University, and CMST COST Action CM1203 (PoCheMoN) for support. M.H. and E.C. thank Labex CHARMMMAT (ANR-11-LBX-0039-grant). D.T. and M.W. thank the German Research Council (DFG) for financial support for the X-ray diffraction setup (INST 1841154-1FUGG). This work was also supported by the Spanish government (CTQ2017-87269-P) and the Generalitat de Catalunya (2017-SGR629). J.M.P. thanks the ICREA foundation for an ICREA ACADEMIA award. F.W. thanks the European Union's Horizon 2020 research programme (Marie Skłodowska-Curie grant No. 713679) for a PhD fellowship. The authors declare no competing financial interests. Figures 1, 2, and 4 were generated by Diamond, Version 3.2 (copyright Crystal Impact GbR). Open access funding enabled and organized by Projekt DEAL.

Conflict of interest

The authors declare no conflict of interest.

Keywords: inorganic chemistry · neutral clusters · organic–inorganic frameworks · polyoxopalladium · supramolecular chemistry

[1] a) C. F. Baes, R. E. Mesmer, *The Hydrolysis of Cations*, Krieger, Malabar, **1986**; b) A. T. Wagner, P. W. Roesky, *Eur. J. Inorg. Chem.* **2016**, 782 – 791.

[2] a) G. Rajaraman, M. Murugesu, E. C. Sañudo, M. Soler, W. Wernsdorfer, M. Helliwell, C. Muryn, J. Raftery, S. J. Teat, G. Christou, E. K. Brechin, *J. Am. Chem. Soc.* **2004**, *126*, 15445 – 15457; b) L. F. Jones, G. Rajaraman, J. Brockman, M. Murugesu, E. C. Sañudo, J. Raftery, S. J. Teat, W. Wernsdorfer, G. Christou, E. K. Brechin, D. Collison, *Chem. Eur. J.* **2004**, *10*, 5180 – 5194; c) N. E. Chakov, W. Wernsdorfer, K. A. Abboud, G. Christou, *Inorg. Chem.* **2004**, *43*, 5919 – 5930; d) P. D. W. Boyd, Q. Li, J. B. Vincent, K. Folting, H. R. Chang, W. E. Streib, J. C. Huffman, G. Christou, D. N. Hendrickson, *J. Am. Chem. Soc.* **1988**, *110*, 8537 – 8539; e) C. Boskovic, E. K. Brechin, W. E. Streib, K. Folting, D. N. Hendrickson, G. Christou, *Chem. Commun.* **2001**, 467 – 468; f) D. N. Hendrickson, S. M. J. Aubin, R. C. Squire, K. Folting, W. E. Streib, G. Christou, *Angew. Chem. Int. Ed. Engl.* **1995**, *34*, 887 – 889; *Angew. Chem.* **1995**, *107*, 969 – 971; g) A. J. Tasiopoulos, A. Vinslava, W. Wernsdorfer, K. A. Abboud, G. Christou, *Angew. Chem. Int. Ed.* **2004**, *43*, 2117 – 2121; *Angew. Chem.* **2004**, *116*, 2169 – 2173; h) M. Murrie, *Chem. Soc. Rev.* **2010**, *39*, 1986 – 1995; i) G. J. T. Cooper, G. N. Newton, P. Kögerler, D.-L. Long, L. Engelhardt, M. Luban, L. Cronin, *Angew. Chem. Int. Ed.* **2007**, *46*, 1340 – 1344; *Angew. Chem.* **2007**, *119*, 1362 – 1366; j) G. N. Newton, G. J. T. Cooper, P. Kögerler, D.-L. Long, L. Cronin, *J. Am. Chem. Soc.* **2008**, *130*, 790 – 791; k) D. Gatteschi, R. Sessoli, A. Cornia, *Chem. Commun.* **2000**, 725 – 732.

[3] a) S. Gross, *J. Mater. Chem.* **2011**, *21*, 15853 – 15861; b) U. Schubert, *Coord. Chem. Rev.* **2017**, *350*, 61 – 67; c) Y.-Z. Yu, Y.-R. Zhang, C.-H. Geng, L. Sun, Y. Guo, Y.-R. Feng, Y.-X. Wang, X.-M. Zhang, *Inorg. Chem.* **2019**, *58*, 16785 – 16791; d) W.-H. Fang, L. Zhang, J. Zhang, *J. Am. Chem. Soc.* **2016**, *138*, 7480 – 7483; e) M.-Y. Gao, L. Zhang, J. Zhang, *Chem. Eur. J.* **2019**, *25*, 10450 – 10455; f) L. Geng, C.-H. Liu, S.-T. Wang, W.-H. Fang, J. Zhang, *Angew. Chem. Int. Ed.* **2020**, *59*, 16735 – 16740; *Angew. Chem.* **2020**, *132*, 16878 – 16883.

[4] a) S. Gao, *Molecular Nanomagnets and Related Phenomena*, Springer Berlin Heidelberg, Berlin, **2015**; b) X.-Y. Zheng, M.-H. Du, M. Amiri, M. Nyman, Q. Liu, T. Liu, X.-J. Kong, L.-S. Long, L.-S. Zheng, *Chem. Eur. J.* **2020**, *26*, 1388 – 1395.

[5] W.-H. Fang, L. Zhang, J. Zhang, *Chem. Soc. Rev.* **2018**, *47*, 404 – 421.

[6] a) M. D. Kärkäs, B. Åkermark, *Dalton Trans.* **2016**, *45*, 14421 – 14461; b) R. Al-Oweini, A. Sartorel, B. S. Bassil, M. Natali, S. Berardi, F. Scandola, U. Kortz, M. Bonchio, *Angew. Chem. Int. Ed.* **2014**, *53*, 11182 – 11185; *Angew. Chem.* **2014**, *126*, 11364 – 11367; c) M. Natali, I. Bazzan, S. Goberna-Ferrón, R. Al-Oweini, M. Ibrahim, B. S. Bassil, H. Dau, F. Scandola, J. R. Galán-Mascarós, U. Kortz, A. Sartorel, I. Zaharieva, M. Bonchio, *Green Chem.* **2017**, *19*, 2416 – 2426.

[7] a) Z. Zheng, *Recent Development in Clusters of Rare Earths and Actinides: Chemistry and Materials*, Springer Berlin Heidelberg, Berlin, **2016**; b) J.-B. Peng, Q.-C. Zhang, X.-J. Kong, Y.-Z. Zheng, Y.-P. Ren, L.-S. Long, R.-B. Huang, L.-S. Zheng, Z. Zheng, *J. Am. Chem. Soc.* **2012**, *134*, 3314 – 3317.

[8] a) P. C. Andrews, W. J. Gee, P. C. Junk, M. Massi, *New J. Chem.* **2013**, *37*, 35 – 48; b) D. N. Woodruff, R. E. P. Winpenny, R. A. Layfield, *Chem. Rev.* **2013**, *113*, 5110 – 5148.

[9] a) Z.-E. Lin, G.-Y. Yang, *Eur. J. Inorg. Chem.* **2011**, 3857 – 3867; b) Z.-E. Lin, G.-Y. Yang, *Eur. J. Inorg. Chem.* **2010**, 2895 – 2902; c) C. Falaise, K. Kozma, M. Nyman, *Chem. Eur. J.* **2018**, *24*, 14226 – 14232; d) Z. Li, L.-D. Lin, H. Yu, X.-X. Li, S.-T. Zheng, *Angew. Chem. Int. Ed.* **2018**, *57*, 15777 – 15781; *Angew. Chem.* **2018**, *130*, 16003 – 16007; e) J.-H. Liu, L.-D. Lin, G.-Q. Wang, L.-Y. Li, Y.-Q. Sun, X.-X. Li, S.-T. Zheng, *Chem. Commun.* **2020**, *56*, 10305 – 10308.

[10] a) S. Yuan, J.-S. Qin, C. T. Lollar, H.-C. Zhou, *ACS Cent. Sci.* **2018**, *4*, 440 – 450; b) C. Xu, Y. Pan, G. Wan, H. Liu, L. Wang, H. Zhou, S.-H. Yu, H.-L. Jiang, *J. Am. Chem. Soc.* **2019**, *141*, 19110 – 19117; c) S. Yuan, J.-S. Qin, H.-Q. Xu, J. Su, D. Rossi, Y. Chen, L. Zhang, C. Lollar, Q. Wang, H.-L. Jiang, D. H. Son, H. Xu, Z. Huang, X. Zou, H.-C. Zhou, *ACS Cent. Sci.* **2018**, *4*, 105 – 111; d) A. A. Bezrukov, K. W. Törnroos, E. Le Roux, P. D. C. Dietzel, *Chem. Commun.* **2018**, *54*, 2735 – 2738; e) L. Qin, H.-G. Zheng, *CrystEngComm* **2017**, *19*, 745 – 757; f) L.-D. Lin, D. Zhao, X.-X. Li, S.-T. Zheng, *Chem. Eur. J.* **2019**, *25*, 442 – 453; g) S. Bhattacharya, W. W. Ayass, D. H. Taffa, A. Schneemann, A. L. Semrau, S. Wannapaiboon, P. J. Altmann, A. Pöthig, T. Nisar, T. Balster, N. C. Burtch, V. Wagner, R. A. Fischer, M. Wark, U. Kortz, *J. Am. Chem. Soc.* **2019**, *141*, 3385 – 3389; h) S. Bhattacharya, M. Gnanavel, A. J. Bhattacharyya, S. Natarajan, *Cryst.*

 © 2020 The Authors. Angewandte Chemie International Edition published by Wiley-VCH GmbH

Growth Des. **2014**, *14*, 310 – 325; i) S. Bhattacharya, A. J. Bhattacharyya, S. Natarajan, *Inorg. Chem.* **2015**, *54*, 1254 – 1271.

[11] a) M. Pope, Y. Jeannin, M. Fournier, *Heteropoly and Isopoly Oxometalates*, Springer Berlin Heidelberg, **1983**; b) M. T. Pope, A. Müller, *Angew. Chem. Int. Ed. Engl.* **1991**, *30*, 34 – 48; *Angew. Chem.* **1991**, *103*, 56 – 70.

[12] a) V. W. Day, W. G. Klemperer, *Science* **1985**, *228*, 533; b) Issue dedicated to Polyoxometalates (Guest Ed.: U. Kortz): *Eur. J. Inorg. Chem.* **2009**, *34*; c) A. Dolbecq, E. Dumas, C. R. Mayer, P. Mialane, *Chem. Rev.* **2010**, *110*, 6009 – 6048; d) N. Mizuno, K. Kamata, *Coord. Chem. Rev.* **2011**, *255*, 2358 – 2370; e) L. E. Briand, G. T. Baronetti, H. J. Thomas, *Appl. Catal. A* **2003**, *256*, 37 – 50; f) E. Coronado, C. Giménez-Saiz, C. J. Gómez-García, *Coord. Chem. Rev.* **2005**, *249*, 1776 – 1796; g) M. T. Pope, A. Müller, *Polyoxometalates: From Platonic Solids to Anti-Retroviral Activity*, Springer, Dordrecht, **2012**; h) U. Kortz, A. Müller, J. van Slageren, J. Schnack, N. S. Dalal, M. Dressel, *Coord. Chem. Rev.* **2009**, *253*, 2315 – 2327; i) D.-L. Long, E. Burkholder, L. Cronin, *Chem. Soc. Rev.* **2007**, *36*, 105 – 121; j) D.-L. Long, R. Tsunashima, L. Cronin, *Angew. Chem. Int. Ed.* **2010**, *49*, 1736 – 1758; *Angew. Chem.* **2010**, *122*, 1780 – 1803; k) A. Müller, P. Gouzerh, *Chem. Soc. Rev.* **2012**, *41*, 7431 – 7463; l) R. Liu, G. Zhang, H. Cao, S. Zhang, Y. Xie, A. Haider, U. Kortz, B. Chen, N. S. Dalal, Y. Zhao, L. Zhi, C.-X. Wu, L.-K. Yan, Z. Su, B. Keita, *Energy Environ. Sci.* **2016**, *9*, 1012 – 1023.

[13] a) S. S. Mal, U. Kortz, *Angew. Chem. Int. Ed.* **2005**, *44*, 3777 – 3780; *Angew. Chem.* **2005**, *117*, 3843 – 3846; b) A. H. Ismail, B. S. Bassil, G. H. Yassin, B. Keita, U. Kortz, *Chem. Eur. J.* **2012**, *18*, 6163 – 6166; c) P. Yang, M. Alsufyani, A.-H. Emwas, C. Chen, N. M. Khashab, *Angew. Chem. Int. Ed.* **2018**, *57*, 13046 – 13051; *Angew. Chem.* **2018**, *130*, 13230 – 13235; d) T. Boyd, S. G. Mitchell, D. Gabb, D.-L. Long, Y.-F. Song, L. Cronin, *J. Am. Chem. Soc.* **2017**, *139*, 5930 – 5938; e) S. Uchida, N. Mizuno, *Coord. Chem. Rev.* **2007**, *251*, 2537 – 2546.

[14] a) J. W. Döbereiner, *J. Chem. Phys.* **1828**, *54*, 412 – 426; b) J. C. Goloboy, W. G. Klemperer, *Angew. Chem. Int. Ed.* **2009**, *48*, 3562 – 3564; *Angew. Chem.* **2009**, *121*, 3614 – 3616.

[15] M. Pley, M. S. Wickleder, *Angew. Chem. Int. Ed.* **2004**, *43*, 4168 – 4170; *Angew. Chem.* **2004**, *116*, 4262 – 4264.

[16] a) P. Yang, U. Kortz, *Acc. Chem. Res.* **2018**, *51*, 1599 – 1608; b) E. V. Chubarova, M. H. Dickman, B. Keita, L. Nadjo, F. Miserque, M. Mifsud, I. W. C. E. Arends, U. Kortz, *Angew. Chem. Int. Ed.* **2008**, *47*, 9542 – 9546; *Angew. Chem.* **2008**, *120*, 9685 – 9689; c) M. Barsukova, N. V. Izarova, R. N. Biboum, B. Keita, L. Nadjo, V. Ramachandran, N. S. Dalal, N. S. Antonova, J. J. Carbó, J. M. Poblet, U. Kortz, *Chem. Eur. J.* **2010**, *16*, 9076 – 9085; d) P. Yang, Y. Xiang, Z. Lin, B. S. Bassil, J. Cao, L. Fan, Y. Fan, M.-X. Li, P. Jiménez-Lozano, J. J. Carbó, J. M. Poblet, U. Kortz, *Angew. Chem. Int. Ed.* **2014**, *53*, 11974 – 11978; *Angew. Chem.* **2014**, *126*, 12168 – 12172; e) N. V. Izarova, N. Vankova, A. Banerjee, G. B. Jameson, T. Heine, F. Schinle, O. Hampe, U. Kortz, *Angew. Chem. Int. Ed.* **2010**, *49*, 7807 – 7811; *Angew. Chem.* **2010**, *122*, 7975 – 7980; f) M. Barsukova-Stuckart, N. V. Izarova, G. B. Jameson, V. Ramachandran, Z. Wang, J. van Tol, N. S. Dalal, R. Ngo Biboum, B. Keita, L. Nadjo, U. Kortz, *Angew. Chem. Int. Ed.* **2011**, *50*, 2639 – 2642; *Angew. Chem.* **2011**, *123*, 2688 – 2692; g) F. Xu, H. N. Miras, R. A. Scullion, D.-L. Long, J. Thiel, L. Cronin, *Proc. Natl. Acad. Sci. USA* **2012**, *109*, 11609.

[17] a) N. V. Izarova, R. N. Biboum, B. Keita, M. Mifsud, I. W. C. E. Arends, G. B. Jameson, U. Kortz, *Dalton Trans.* **2009**, 9385 – 9387; b) W. W. Ayass, J. F. Miñambres, P. Yang, T. Ma, Z. Lin, R. Meyer, H. Jaensch, A.-J. Bons, U. Kortz, *Inorg. Chem.* **2019**, *58*, 5576 – 5582.

[18] a) N. V. Izarova, N. Vankova, T. Heine, R. N. Biboum, B. Keita, L. Nadjo, U. Kortz, *Angew. Chem. Int. Ed.* **2010**, *49*, 1886 – 1889; *Angew. Chem.* **2010**, *122*, 1930 – 1933; b) Y. Xiang, N. V. Izarova, F. Schinle, O. Hampe, B. Keita, U. Kortz, *Chem. Commun.* **2012**, *48*, 9849 – 9851; c) N. V. Izarova, A. Kondinski, N. Vankova, T. Heine, P. Jäger, F. Schinle, O. Hampe, U. Kortz, *Chem. Eur. J.* **2014**, *20*, 8556 – 8560.

[19] P. Yang, Y. Xiang, Z. Lin, Z. Lang, P. Jiménez-Lozano, J. J. Carbó, J. M. Poblet, L. Fan, C. Hu, U. Kortz, *Angew. Chem. Int. Ed.* **2016**, *55*, 15766 – 15770; *Angew. Chem.* **2016**, *128*, 15998 – 16002.

[20] a) Z. Wang, F.-L. Yang, Y. Yang, Q.-Y. Liu, D. Sun, *Chem. Commun.* **2019**, *55*, 10296 – 10299; b) Y. Yang, T. Jia, Y.-Z. Han, Z.-A. Nan, S.-F. Yuan, F.-L. Yang, D. Sun, *Angew. Chem.* **2019**, *131*, 12408 – 12413; c) X.-L. Pei, Y. Yang, Z. Lei, S.-S. Chang, Z.-J. Guan, X.-K. Wan, T.-B. Wen, Q.-M. Wang, *J. Am. Chem. Soc.* **2015**, *137*, 5520 – 5525; d) E. L.-M. Wong, R. W.-Y. Sun, N. P. Y. Chung, C.-L. S. Lin, N. Zhu, C.-M. Che, *J. Am. Chem. Soc.* **2006**, *128*, 4938 – 4939; e) S. Chen, W.-H. Fang, L. Zhang, J. Zhang, *Angew. Chem. Int. Ed.* **2018**, *57*, 11252 – 11256; *Angew. Chem.* **2018**, *130*, 11422 – 11426; f) H. E. Toma, K. Araki, A. D. P. Alexiou, S. Nikolaou, S. Dovidauskas, *Coord. Chem. Rev.* **2001**, *219 – 221*, 187 – 234; g) J. R. Houston, M. M. Olmstead, W. H. Casey, *Inorg. Chem.* **2006**, *45*, 7799 – 7805; h) M. Ibrahim, M. H. Dickman, A. Suchopar, U. Kortz, *Inorg. Chem.* **2009**, *48*, 1649 – 1654.

[21] A. Upadhyay, J. Rajpurohit, M. Kumar Singh, R. Dubey, A. Kumar Srivastava, A. Kumar, G. Rajaraman, M. Shanmugam, *Chem. Eur. J.* **2014**, *20*, 6061 – 6070.

[22] a) T. Steiner, *Acta Crystallogr. Sect. B* **1998**, *54*, 456 – 463; b) C. B. Aakeröy, T. A. Evans, K. R. Seddon, I. Pálinkó, *New J. Chem.* **1999**, *23*, 145 – 152; c) M. Ikeda, A. K. Sah, M. Iwase, R. Murashige, J.-i. Ishi-i, M. Hasegawa, C. Kachi-Terajima, K.-M. Park, S. Kuwahara, Y. Habata, *Dalton Trans.* **2017**, *46*, 3800 – 3804; d) C. L. D. Gibb, E. D. Stevens, B. C. Gibb, *J. Am. Chem. Soc.* **2001**, *123*, 5849 – 5850.

[23] a) A. C. Sudik, A. P. Côté, O. M. Yaghi, *Inorg. Chem.* **2005**, *44*, 2998 – 3000; b) G. Yang, R. G. Raptis, *Chem. Commun.* **2004**, 2058 – 2059; c) C. Serre, F. Millange, S. Surblé, G. Férey, *Angew. Chem. Int. Ed.* **2004**, *43*, 6285 – 6289; *Angew. Chem.* **2004**, *116*, 6445 – 6449; d) Y. Cui, H. L. Ngo, P. S. White, W. Lin, *Chem. Commun.* **2002**, 1666 – 1667.

[24] a) R. Atencio, A. Briceño, X. Galindo, *Chem. Commun.* **2005**, 637 – 639; b) C.-H. Zeng, Z. Luo, J. Yao, *CrystEngComm* **2017**, *19*, 613 – 617; c) C. B. Aakeröy, A. M. Beatty, D. S. Leinen, *Angew. Chem. Int. Ed.* **1999**, *38*, 1815 – 1819; *Angew. Chem.* **1999**, *111*, 1932 – 1936.

[25] A. F. Wells, *Three dimensional nets and polyhedra*, Wiley, New York, **1977**.

[26] D. L. Sastry, A. Naito, C. A. McDowell, *Chem. Phys. Lett.* **1988**, *146*, 422 – 427.

[27] a) https://www.sciencedirect.com/topics/agricultural-and-biological-sciences/cacodylic-acid; b) G. M. Bernard, A. Goyal, M. Miskolzie, R. McKay, Q. Wu, R. E. Wasylishen, V. K. Michaelis, *J. Magn. Reson.* **2017**, *283*, 14 – 21.

[28] Y. Jiang, J. Huang, W. Dai, M. Hunger, *Solid State Nucl. Magn. Reson.* **2011**, *39*, 116 – 141.

[29] R. E. Schreiber, L. Houben, S. G. Wolf, G. Leitus, Z.-L. Lang, J. J. Carbó, J. M. Poblet, R. Neumann, *Nat. Chem.* **2017**, *9*, 369 – 373.

[30] a) R. Wilcken, M. O. Zimmermann, A. Lange, A. C. Joerger, F. M. Boeckler, *J. Med. Chem.* **2013**, *56*, 1363 – 1388; b) A. Priimagi, G. Cavallo, P. Metrangolo, G. Resnati, *Acc. Chem. Res.* **2013**, *46*, 2686 – 2695.

[31] I. Chakraborty, T. Pradeep, *Chem. Rev.* **2017**, *117*, 8208 – 8271.

Manuscript received: August 7, 2020
Revised manuscript received: October 23, 2020
Accepted manuscript online: October 26, 2020
Version of record online: December 15, 2020

 © 2020 The Authors. Angewandte Chemie International Edition published by Wiley-VCH GmbH